

RSC Advances



This is an *Accepted Manuscript*, which has been through the Royal Society of Chemistry peer review process and has been accepted for publication.

Accepted Manuscripts are published online shortly after acceptance, before technical editing, formatting and proof reading. Using this free service, authors can make their results available to the community, in citable form, before we publish the edited article. This *Accepted Manuscript* will be replaced by the edited, formatted and paginated article as soon as this is available.

You can find more information about *Accepted Manuscripts* in the [Information for Authors](#).

Please note that technical editing may introduce minor changes to the text and/or graphics, which may alter content. The journal's standard [Terms & Conditions](#) and the [Ethical guidelines](#) still apply. In no event shall the Royal Society of Chemistry be held responsible for any errors or omissions in this *Accepted Manuscript* or any consequences arising from the use of any information it contains.

ARTICLE

Solution Processed Transparent Nanoparticulate ZnO Thin Film Electrode for Photoelectrochemical Water Oxidation

Cite this: DOI: 10.1039/x0xx00000x

Debajeet K. Bora ^a, Artur Braun ^{a*}

Received 00th January 2012,
Accepted 00th January 2012

DOI: 10.1039/x0xx00000x

www.rsc.org/

A non-aqueous solution processing route followed by dip-coating has been developed to deposit ZnO thin film with average nanoparticles size of 21.04 nm. The optical, morphological and structural characterization of the film is studied in order to confirm its band gap, particle size distribution and crystallographic properties. Finally the photoelectrochemical of studies of different layers deposited ZnO films has shown that the optimized film for 2 layers deposition at 500°C exhibit anodic photocurrent density 1 mA / cm² without any modification. Surprisingly the photocurrent density at water splitting potential 1.23 V is quite high with a magnitude of 0.817 mA / cm². The photocurrent experiment is followed by chopped light investigation in order to have information about the charge transfer characteristics and here the absence of cathodic spike rules out any recombination effect in the bulk of ZnO electrode. In this study, we also propose that this kind of transparent electrode having photoelectrochemical functionality can be used as a large window panel in modern household with the aim of performing dual purpose work: UV filtering and photoelectrochemical water splitting. The evolved oxygen by the electrode is further quantitated with in-situ gas chromatographic study.

A Introduction

The photoelectrochemical (PEC) water oxidation is one of the key steps of photoelectrochemical water splitting taking place on semiconductors and works on the principle of semiconductor electrochemistry [1]. The chemistry associated within the process leads to the formation of oxygen and hydrogen gases which can be used as future green fuel to fulfil the energy demands. To accomplish it, one needs solar photons and suitable amount of electrical bias to a semiconductor electrode in an electrochemical environment having ionic conductivity. The effect of light on electrochemical experiment was first validated by Becquerel [2]. The photoelectrochemical water splitting on semiconductor electrode was first accomplished by Fujishima and Honda in 1972 on n-Type TiO₂ electrode with an efficiency of 0.1% [3]. The use of metal oxide for PEC water splitting process was very helpful with respect to its semiconducting properties such as ability to absorb sunlight, stability in neutral and basic environment, non – toxicity and earth abundance. Based on these advantages, hematite was first used as a photoanode to study its water oxidation properties by Hardee and Bard and they found a low efficiency due to its short hole diffusion length as noted by Gärtner [4, 5]. Besides hematite, numerous other metal oxides have also been tested to

study its photo-oxidative behaviour [6]. Of these, ZnO semiconductors have been found effective as a photoanode for water splitting reaction due to its electrochemical stability and electron mobility [7]. In this case, Tributsch and Calvin for the first time sensitized the surface of ZnO single crystal with chlorophyll molecule and found that on exciting it with light, electrons were injected to the conduction band of semiconductor from dye molecule resulted in anodic photocurrent [8]. ZnO is still used nowadays as photoanode for water splitting reaction in various morphological forms such as nanowire, nanorod and nanoparticulate films [9 – 11]. However due to its wide band gap (3.2 eV) [12], it is not suitable for absorbing the visible light photons. In order to make it effective for PEC application, studies have been carried out to tune its electronic band gap with doping, quantum dot sensitization, dye sensitization and surface functionalization of bent ZnO nanorod with Ag nanoparticle [13- 21]. In another route, the efficiency of ZnO electrode is further improved with Cobalt co - catalyst treatment [22]. Apart from the PEC application, ZnO has many different uses in the areas of solar cells, organic photovoltaic, thin films transistors, quantum dots, biomedical applications, as heterogeneous industrial catalysts for methanol production etc. [23-28]. Coming back to the effectiveness of ZnO electrode, if we look into its electronic energy level

diagram as depicted elsewhere [29], its conduction band situated above water reduction potential and hence will need less applied bias or overpotential in contrary to hematite. ZnO photoanode mentioned above are prepared by various methods: viz. spray pyrolysis, hydrothermal methods, atomic layer deposition, pulsed laser deposition, RF magnetron sputtering, electron beam evaporation etc. [30, 31, 24, 11, 13, 21].

Solution processed ZnO thin films are also find an added advantage due to its transparent nature [32, 25]. The electrode obtained in this manner can be applicable as a PEC integrated window in modern households. The solution processed technique enabled the production of thin film by mass manufacturing with the help of roll to roll processing using conventional dip-coating, doctor blade, screen printing etc. [25, 33]. Another advantage of solution processing route is the low cost and can be utilized further for large area panel fabrication [34]. Due to the non-toxicity and environmental stability [25], it is user friendly as a PEC integrated window in household. The solution processed ZnO photoanode in pristine state has not been studied a lot and the photocurrent density obtained in the above cases is not so high. The best anodic photocurrent density obtained with PLD (pulsed laser deposition) deposited pristine nanoparticulate film [11] was $200\mu\text{A}/\text{cm}^2$. In another study, the cathodic photocurrent density reported was $1\text{ mA}/\text{cm}^2$ for an non-doped ZnO electrode [35]. In this regard, reactive magnetron sputtering gives rise to some compact film with transparent nature. But this is used mostly for solar cell application. A comparison of photoelectrochemical properties of different ZnO photoelectrodes is summarized in Table 1.

In the current study, our goal is to develop an effective solution processing route to obtain high quality transparent ZnO films so that it can be used as a PEC integrated window with dual functionality: UV filter and photoelectrochemical water splitting. Here, we have described an effective non - aqueous solution processing route for getting ZnO nanoparticulate thin film with improved anodic photocurrent density even in pristine condition and which we believe is quite high comparing to others as depicted in Table I.

B Experimental

Materials and methods

All precursors: $\text{Zn}(\text{NO}_3)_2 \cdot 4\text{H}_2\text{O}$, oleic acid and tetra hydro furan (THF) used in this study were obtained from Aldrich and used without further purification. Fluorine doped tin oxide (FTO) used for depositing ZnO film was from Pilkington Glass Inc., U.K. and had a sheet resistance of $5.5\Omega\text{cm}^{-1}$.

Synthesis Procedures

ZnO thin films have been synthesized by adopting a non - aqueous processing route. In the first step of the synthesis process, 18 gm. of oleic acid have been taken in a beaker

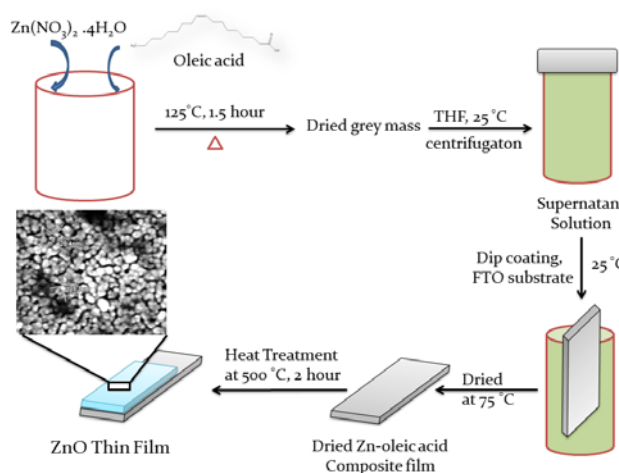
Table 1: Photocurrent densities of various ZnO electrodes prepared with different methods

Photoelectrode	Deposition method	Photocurrent density	Reference
ZnO and Fe doped ZnO	Sol-gel and spin-coating method	$1\text{ mA}/\text{cm}^2$, Remark: P-type semiconductor, cathodic photocurrent	[35]
Cobalt deposited ZnO	Electrodeposition	$0.02\text{ mA}/\text{cm}^2$	[22]
N- doped ZnO and Al, N co - doped ZnO	Radiofrequency magnetron sputtering	$0.03\text{ mA}/\text{cm}^2$	[15]
ZnO nanocorral	Thermal oxidation, RF magnetron sputtering	$0.05\text{ mA}/\text{cm}^2$	[48]
ZnO nanostructured film	Pulsed laser deposition	$0.2\text{ mA}/\text{cm}^2$	[11]
ZnO nanorod	Hydrothermal deposition	$5\text{mA}/\text{cm}^2$	[31]
N- doped ZnO wire	Hydrothermal deposition followed by annealing in the presence of NH_3	$0.5\text{mA}/\text{cm}^2$	[9]
ZnO nanostructured film	Solution processing and dip-coating	$1\text{ mA}/\text{cm}^2$	This study

and melt it over a hot plate at 100°C . After this 28 gm. of $\text{Zn}(\text{NO}_3)_2 \cdot 4\text{H}_2\text{O}$ have been added with consequent stirring at 125°C . The mixture have been heated up to 1.5 hour till all Zinc salt gets decomposed and evolves out all the residual NO_2 gas from the reaction mixture. After this step, a dried grey mass has been obtained and consequently treated with 80 ml of THF (tetra hydro furan) to make dispersion. The dispersion has been further centrifuged (5000 rpm for 4 min) to get supernatant solution as depicted in scheme I. The supernatant solution containing Zinc - oleate mixture has been kept further for thin film deposition with dip-coating process.

The ZnO thin film has been obtained by adopting the methodology as described follows: First, FTO coated glass have been cleaned with soap water, acetone and iso - propyl alcohol and make it dry at room temperature. After this the FTO substrates have been dip-coated in the supernatant solution with 1 layer and dried at 75°C on a hot plate. The dried dip-coated film has been further subjected to heat treatment process at 500°C for dwelling time of 30 min. After this, the ZnO thin film has been cooled down at room temperature and further studied with UV-Vis, XRD, FESEM, EDX and photocurrent density measurement.

The optimization of films thickness and heat treatment process has been carried out further in order to have best functional film with highest photocurrent density. After dip-coating treatment, film has been optimized for heat treatment temperature. Three different FTO substrates have been given one time dip-coating each so that 1 layer gets deposited and heat treated further at 300 / 400 / 500°C. Photocurrent densities measurement for each of the heat treated films having 1 layer has been carried out. After getting the photocurrent data from heat treated sample we have fixed the temperature at 500 °C and optimized films thickness by giving 1 layer / 2 layers / 3 layers coating to each of the samples at 500 °C. The structural properties of optimized films under different conditions were further characterized with XRD. After this, films have been characterized with profilometry in order to know its thickness. From the optimization process, it is found that 2 layers dip-coated film (thickness 40 nm) with 500°C heat treatment temperature shows highest photocurrent density.



Scheme 1 synthesis steps for getting nanoparticulate ZnO film in solution processed manner.

Characterization

Cary Scan 50 UV-Vis spectrometer was used for determining the optical properties of the ZnO films. The thickness has been determined with a stylus profilometer (Ambios XP-100). XRD measurement was carried out with diffractometer from PAN analytical X'Pert PRO having $\text{CuK}\alpha$ radiation. The morphology of film and composition has been studied with FESEM and EDX (Hitachi S-4800 model equipped with EDX spectrometer from Oxford instruments). For the photoelectrochemical water oxidation study, films have been subjected to dark and photocurrent measurements with Voltalab 80 potentiostat in a three-electrode configuration (cappuccino cell) in 1M K_2SO_4 (pH = 6.08) electrolyte. The reference electrode was a calomel electrode ($\text{Hg} / \text{Hg}_2\text{SO}_4 / \text{saturated } \text{K}_2\text{SO}_4$) and a platinum wire used as counter-electrode. Photoelectrochemical studies were performed by illuminating the ZnO film through a 0.45 cm^2 aperture window of the electrode through a fused silica window with a 0.5 cm^2 circular

mask; the total geometric area immersed in the electrolyte was approximately 2.6 cm^2 . Sunlight was simulated with a filtered xenon lamp from LOT® Oriol. The light intensity was adjusted to AM 1.5 simulated lights using a THORLABS Inc. energy meter.

C Results and discussion

Synthesis and optical properties of the prepared film

The dip-coated ZnO film obtained at 500°C is transparent in nature and is as shown in left side of Figure 1. Visual inspection of the film reveals different colour contrast due to interference fringes which can also be seen in case of an ultra-thin Ge film on Au substrate [36]. The optical microscopy of the film [Figure 1: Right] shows the formation of topological patterns formation after dip-coating and heat treatment process. The non-aqueous processing route for precursor synthesis involves the formation of zinc - oleate composite. The composite consists of Zn ion distributed in oleic acid matrix. On annealing at 500°C oleate gets thermally decompose and Zn ion is oxidized into ZnO. The prepared ZnO thin film is very compact and don't have any cracks as observed in an earlier case of making pristine hematite film by following the same route [37]. So far we have discussed the synthesis process and visual properties of the film. To get a detail understanding of the film and its functionality, it has been further characterized with different auxiliary tools. In this case we have studied the effects of two different parameters on ZnO film properties viz. number of dip-coated layers and heat treatment temperatures.

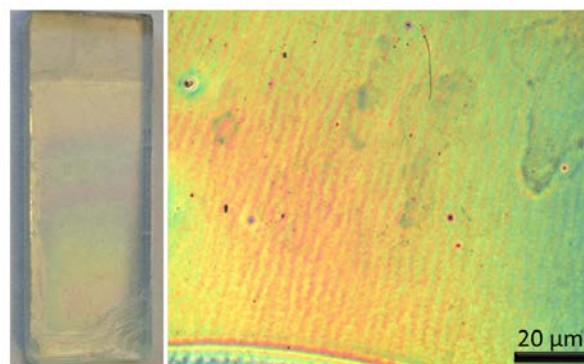


Figure 1: Left. Optimized ZnO film image showing colour contrast as a result of interference fringes; Right. Optical microscopy of ZnO films at $20 \mu\text{m}$ resolution showing the presence of topological pattern.

The optical properties of the nanoparticulate film largely determine its functionality as a photoanode for photoelectrochemical water oxidation. This is due to the band gap and electronic structure of the electrode material which plays a critical role to make it more effective for photoelectrochemical water splitting. The band gap determines the type of solar insolation to be absorbed by the material. In this case, ZnO absorbed mostly UV portion of solar spectrum [12] and its conduction band edge position against water reduction potential favours water splitting reaction quite easily

[29] and consequently needs less overpotential for running photo-oxidation reaction as will be discussed below. The UV-Vis transmittance spectrum of the three differently deposited films is shown in Figure 2 A. From it, it is evident that one layer deposited film has an absorbance at 357 nm and is totally transparent in the visible region from 390 nm to 750 nm. This result agrees well with that of solution processed ZnO thin film obtained at 500°C [25]. In case of two layers deposited film (thickness 40 nm), we have observed that the absorption band slightly red shifted towards 378 nm and transparent in visible region. In both cases, the transmittance spectra reveals the formation of interference fringes which is absent in case of three layer deposited film with same absorption edge as that of two layer films. Note that ZnO films used in this investigation are heat treated at 500°C. The shifting of absorption onset can be corroborated with various sizes of nanoparticles constituting the film when we consider different layer thickness. In this case we can bring the concept of quantum size confinement as the thin film has nanoparticles with sizes < 30 nm as can be observed in the discussion of morphological study.

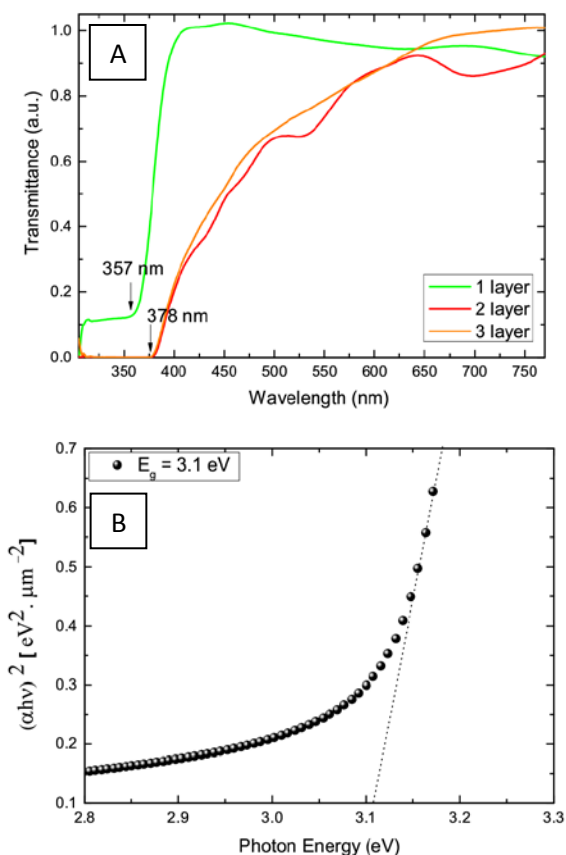


Figure 2: A. UV- Vis transmittance spectrum of ZnO film having different layer thickness showing 90% transmittance for visible region of solar spectrum. B. Energy band gap of ZnO obtained using Tauc model for direct band gap transition.

To get further insight into the electronic structure, the band gap of ZnO thin film has been calculated by applying Tauc methodology [38] for direct band gap transition. Note that n-

type ZnO has a direct band gap of 3.20 eV [12]. From Figure 2 B we have found that ZnO band gap is around 3.13 eV for 2 layers deposited films which generally shows highest photocurrent density in the present study. This will be discussed further in photoelectrochemical properties of ZnO electrode. The observed band gap closely matches with that of ZnO film already described in literatures and the result was explained on the basis of valance band donor transition [12]. The higher band gap of ZnO is attributed to the deeper lying of O 2p and Zn 3d orbitals and studies has been carried out in order to reduce the band gap and to shift the valance band maximum to upper energy level [13]. It also refers to the absorbance of short wavelength light for the ZnO film obtained in this case. This will further help in the absorption of UV rays when use as a smart window system in modern building.

So far from optical property investigation, we have found that the synthesized ZnO thin film is well matching with the standard one already described in literature and due to its UV absorption properties; it further validated the proof of concept of using it as a smart transparent window.

Structural and morphological characteristics of the ZnO films

For the photoelectrochemical application, not only the optical properties; the structural properties equally plays an important role as it gives information about the crystallographic properties of the electrode. This finally determines the electron transport characteristics through the crystalline lattice having right structure and symmetry. To deal with it, we have performed X-ray diffraction study on the thin film of ZnO for two different parameters. In the first case, we have taken account of the effect of heat treatment temperature on its structural properties. Here, we have normalized the ZnO Bragg reflection peak intensity with that of FTO substrate and plotted in Figure 3A. From here, it has been observed that the ZnO film on FTO substrate showing intensity patterns from corresponding crystallographic planes. These are not well resolve in case of 300 and 400 °C, whereas distinct for 500 °C treated film. Here (100), (002), (101) and (103) crystal planes are observed which corresponds well to the JCPDS pattern (01-089-7102) for ZnO with hexagonal phase with space group P63mc [39]. Based on results, it is evident that the substrate (FTO) peak intensity remain same for all films heat treated at different temperatures while the corresponding Bragg reflection peak intensity of ZnO crystalline planes well evolved for 500°C heat treated sample. Based on this, we can conclude that 500°C is the best temperature for obtaining the thin film of ZnO. From the expanded diffractogram of 500 °C [Figure 3 B], it is observed that the peak broadening also occurs for (100), (101) along with (002) planes. This further confirms the formation of nanocrystalline phases and is validates nanoparticles sizes of 21.04 nm as will be discussed in morphology study.

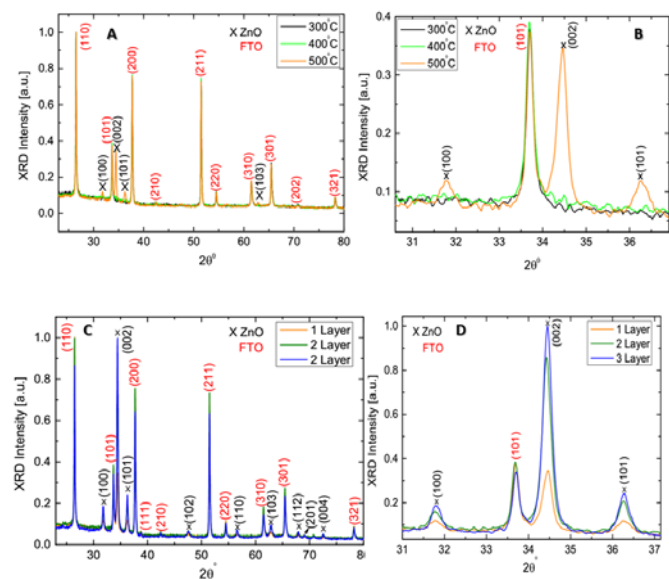


Figure 3: A. XRD study of differently heat treated sample; B. expanded form of XRD pattern showing the presence of ZnO crystalline plane with broadening of Bragg peak; C. thickness dependent XRD study of ZnO heat treated at 500 °C; D. Expanded pattern shows the evolution of Bragg peak intensity for (002) plane followed by others.

Next we have performed X - ray diffraction on ZnO films having different number of dip-coated layers. From Figure 3 C, the Bragg reflection peaks for ZnO are well resolved for all the deposited layers. Here, we have also observed corresponding Bragg reflection patterns from (102), (110), (112), (201), and (004) crystallographic planes in addition to ones discussed above. Note that all XRD characterized films have been deposited at the optimized heat treatment temperature of 500 °C. On expanding the diffractogram between 31° - 37° Bragg angle [Figure 3D.] we have observed that the (002) plane shows its maximum Bragg reflection peak intensity while substrate peak intensity remain invariant for all the films having 1, 2 and 3 layers deposition. From a careful analysis, we have found that the Bragg peak gets broadened more in case of 2 and 3 layers deposited film in comparison to 1 layer film which corresponds to formation of nanocrystallites. We have also observed that although the (002) plane intensity reached its peak maximum but contrary to this, all the planes (100) and (101) intensities getting increase with respect to substrate peak intensity and this rules out any preferential growth of ZnO crystallographic planes on increasing the number of dip-coated layers. While in other cases, (002) planes preferentially grows as described elsewhere [25, 32]. To confirm the preferential growth of crystallographic pattern we have also calculated the relative Bragg peak ratio between (101), (100) and (002) planes of ZnO with that of FTO (101) plane

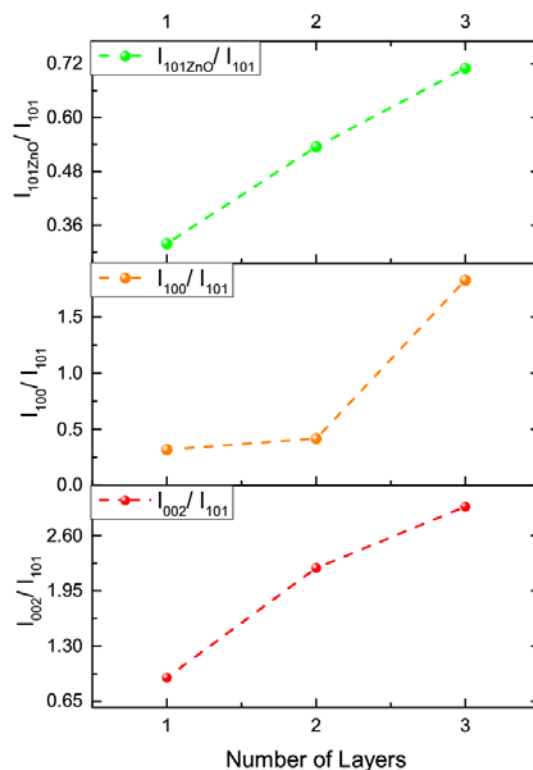


Figure 4: Relative Bragg peak ratio between (101), (100) and (002) planes of ZnO with that of FTO (101) plane.

As shown in Figure 4, we have found that all Bragg reflection peak intensity for crystalline planes of ZnO equally grows at the expense of the layer thickness. Following this discussion, we can conclude the formation of ZnO thin film with hexagonal structure as exemplified by the correct matching to JCPDS intensity patterns. In the next part, we would like to discuss about the morphology study of ZnO thin film. This is important as the morphology plays an important role in the light trapping during solar insolation. Before discussing the morphological data, we would like to point out here that the ZnO film shows higher performance in spite of having compact form with shiny faces as shown in Figure 1 (left). This particular feature was absent in our earlier study for a compact hematite film prepared with spin-coating and sol – gel protocol¹. The current ZnO film is effective in the sense of having roughness at nanoscale which can be observed from the corresponding FESEM images as shown in Figure 5 A and B. From here, it is evident that the film consists of nanoparticles having different diameter and elongated shape. On calculating the Feret's diameter [40] of the elongated nanoparticle, $\langle F \rangle$ with Image J software as shown in Figure 5 D, the average nanoparticle size obtained is around 21.04 nm. This is quite surprising as the same synthesis process for hematite thin film deposition does not allow us to obtain such small nanoparticle sizes [37]. It is also remarkable in the sense of the easy scalability of the synthetic process for depositing ZnO thin films. In addition to it, since the film has roughness at nanoscale, the light trapping improves further which helps in the better photoelectrochemical performance.

The composition of the film has also been studied with EDX spectrometer and it is found that the film consists of only Zn and O elements as can be seen from Figure 5 C. The huge peak before oxygen appears from carbon background which was used as a substrate during the measurement.

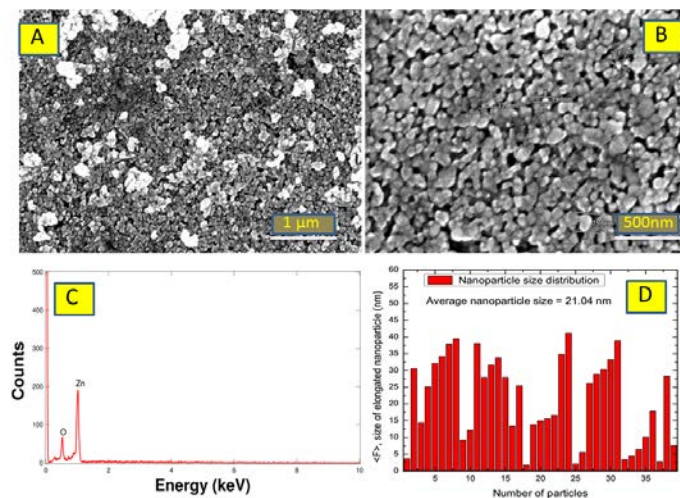


Figure 5: A and B: FESEM images of ZnO film showing nanoparticulate morphology. C. EDX pattern showing the presence of Zn and O elements. D. Average size distribution of nanoparticles constituting the film is 21.04 nm calculated by considering the Feret diameter $\langle F \rangle$ for elongated nanoparticles.

Photoelectrochemical water oxidation

In order to study the functionality of the nanoparticulate ZnO film, we have carried out photoelectrochemical measurement with three - electrode electrochemical configuration with necessary applied bias and in the presence of 1M K_2SO_4 as electrolyte (pH = 6.08), Hg/Hg_2SO_4 (SCE) as reference electrode and Pt as a counter electrode. Before measuring the photocurrent, dark current of the ZnO thin films has been measured to see any faradaic oxidative current. Note that in all electrochemical measurements, the potential is expressed vs. RHE (reversible hydrogen electrode) scale which is obtained by using the following formula.

$$E_{RHE} = E_{Hg/Hg_2SO_4} + 0.059 \times pH + E_{Hg/Hg_2SO_4}^0 = 1.01 \text{ V}; \text{ at } 25^\circ C \quad (1)$$

From the linear current density measurement under both dark and light condition [Figure 6 A.]; we have found that for all the films (1, 2 and 3 layers) the dark current density remains flat and its onset starts at 1650 mV due to Faradaic oxidation reaction. Note that the linear CV measurement is carried out within the potential windows of -800mV to 700 mV vs. Hg/Hg_2SO_4 (SCE) electrode (200 mv to 1700 mV vs. RHE). On the other hand, after measuring the photocurrent with AM 1.5 simulated sunlight; we have found that all the samples show reasonable photocurrent densities.

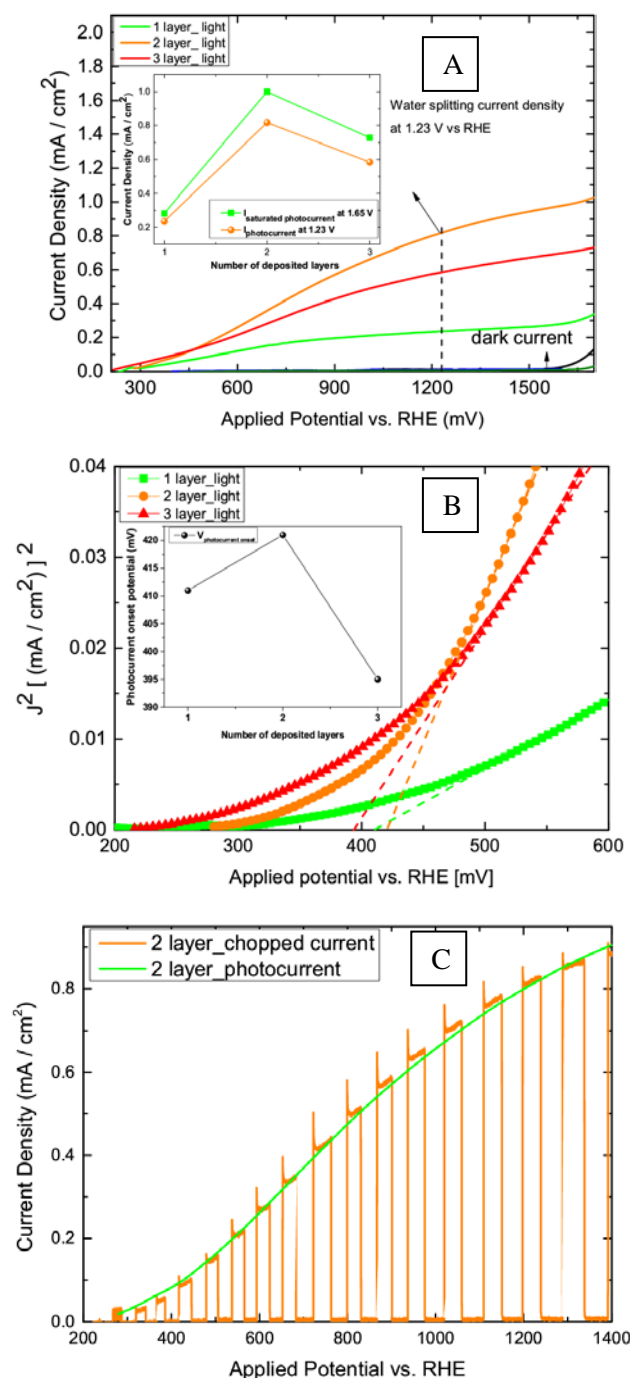


Figure 6: A. Photocurrent densities of ZnO film having different layer of deposition, *inset* showing the variation of saturated photocurrent density and water splitting photo current densities; B. measurement of photocurrent onset potential by plotting square of current density against applied potential ($J^2 - V$); C. Chopped photocurrent density of 2 layer ZnO films showing the presence of anodic spikes tending towards surface recombination of generated electron hole pair.

Here, the 2 layers ZnO film shows the maximum photocurrent density of $1 \text{ mA} / \text{cm}^2$ which is quite high for a pristine ZnO electrode obtained with solution deposition manner in comparison to others as shown in Table 1. However for a P-

type Zn-doped hematite films reasonable amount of photocurrent density was observed [41]. The one layer and three layer films showed photocurrent densities of 0.236 and 0.585 mA / cm² respectively. If we carefully look at the water splitting potential (1.23 V vs. RHE), we have found that the water splitting current density is around 0.817 mA / cm² for 2 layers film which is fairly high. For other films, the variation of water splitting current densities can be visualized from inset of Figure 6 A. Next we have measured the photocurrent onset potentials by making the square of current densities vs. potential [$J^2 - V$ plot] [42] as shown in Figure 6 B. The $J^2 - V$ plot can be used for determining the photocurrent onset potential due to the linear dependence of the square of photocurrent on the applied potential. This helps in the easy determination of photocurrent onset potential by the extrapolation of a straight line to the intersection of applied potential axis. In addition to it, extrapolation of straight line of $J^2 - V$ plot on potential axis can also be used for the determination of flat band potential [43]. Based on the results, it is observed that the photocurrent onset potential for 2 layers film is around 0.421 V with respect to other films as shown in the inset. From the above study, we can conclude here that the 2 layers deposited ZnO film showing the best performance with maximum photocurrent density of 1mA / cm² and photocurrent onset potential starts at 0.421 V. In this case, the overpotential applied is found to be 0.370 V.

To get further understanding of the charge transfer process, we have also performed chopped photocurrent density measurement for 2 layers ZnO film. The result obtained is shown in Figure 6 C. From here, it can be observed that during light on and off condition, anodic spike generated and decays due to the photogeneration of an electron acceptor such as OH• radical during water oxidation reaction and it is generated by the oxidation of water molecule in the electrolyte by valence band holes [44]. The photocurrent generated without any chopping effect (green line) is measured against the potential gradient during which the electrons move from the valence to the conduction band. In this case, another interesting observation is that, no cathodic spike generated during light off condition meaning no recombination taking place between electrons and photo-oxidized surface species in the bulk of electrode [45] and it is quite promising to get rid of recombination effect which generally decreases the efficiency of photoelectrode for water oxidation reaction.

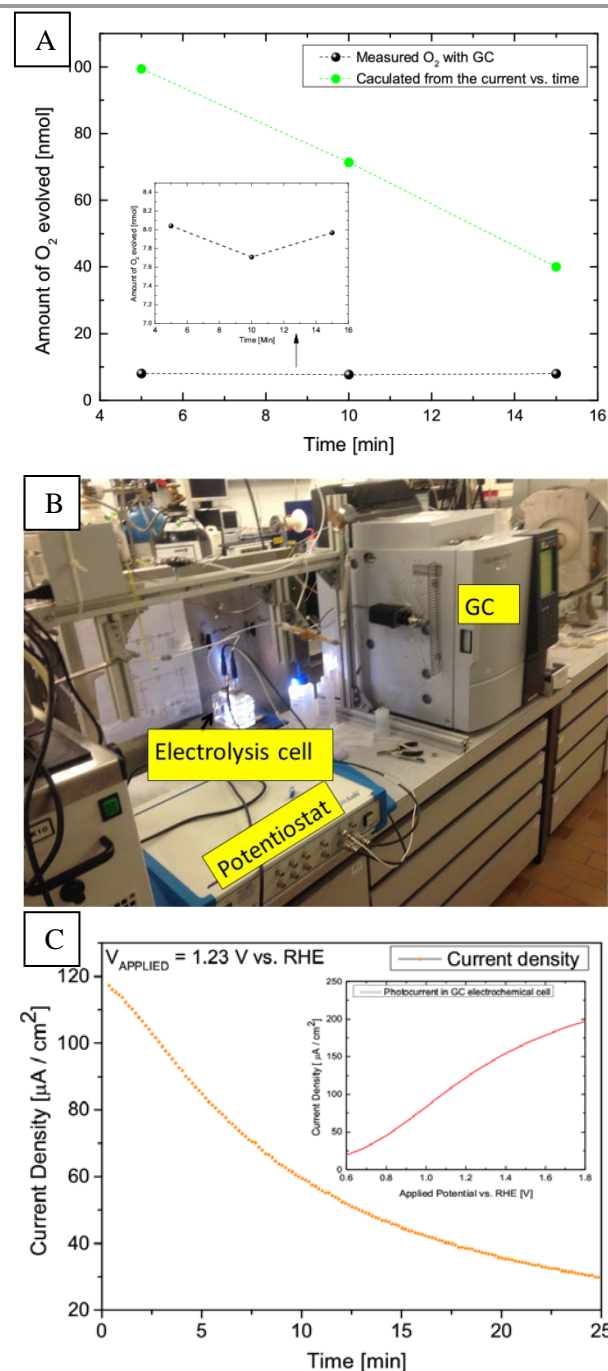


Figure 7. A – Comparison of number of moles of O₂ calculated from current vs. time data with experimentally determined O₂ from GC data analysis. B- measurement set up for in - situ GC detection of photoelectrochemical reaction products. C- Long term stability study in a bulk electrolysis cell; *Inset* showing the measured photocurrent density from one layer deposited ZnO film.

Photoelectrochemical oxygen evolution and stability study

To check the photoelectrochemical oxygen evolution with ZnO film, we have carried out the in - situ gas chromatographic analysis of reaction products (oxygen) formed during the photoelectrochemical experiment. The result obtained is shown in Figure 7 A. Here, we have found that the number of moles of O₂ gets decrease over time as calculated from the

chronoamperometry data using Faradays law [46] and correspondingly the quantitative detection of evolved oxygen yields a concentration of 7.97 nmol after 16 min of the reaction (Figure 7A., inset). The reason for the sharp drop in the O₂ yield after 10 min is not known during this investigation. Also if we carefully look at the chronoamperometry result shown in figure 7 C, after 10 min the photocurrent density drops down to lower value.

Table 2: Experimental and calculated number of moles of evolved O₂

Time	Experimental	Calculated
5 min	8.042 nmol	99.4 nmol
10 min	7.71 nmol	71.4 nmol
15 min	7.97 nmol	40 nmol

We have also calculated the Faradaic efficiency for photoelectrochemical water oxidation with the ZnO film by adopting the method described elsewhere [49]. From the calculation, Faradaic efficiency obtained is around 20% after 15 min of electrode operation. We believe this lower efficiency was due to the occurrence of loss processes in the form of corrosion of electrode surface during the course of experiment. From a rough calculation, we have found that the calculated O₂ after 15 min operation was 40 nmol [Table 2] and it was produced by 160 nmol of electrons. But in case of experimental determination, we have only 7.97 nmol of O₂ which corresponds to 0.5 nmol of electrons. Now if we make a subtraction of the number of mole of electrons, then it will end up with the loss of 159.5 nmol of electrons during the O₂ evolution process which are provided by the current passed over the electrode after 15 min of operation. We believe this loss is due to the corrosion of electrode as confirmed by visual inspection after the photoelectrochemical operation. From the quantitative data, it is evident that the ZnO nanoparticulate film acts as photoanode by forming reaction products in the form of oxygen. This further validates its application as an oxygen generating photoanode. In the next step, we have also studied the long term stability of the ZnO electrode in a bulk electrolysis cell which have been specially designed for the in-situ gas chromatographic detection of reaction products during photoelectrochemical water splitting. The set-up is shown in Figure 7 B.

For the stability study, we have carried out chronoamperometric study of one layer deposited ZnO film for 30 min by employing a fixed potential at 1.23 V vs. RHE. From the current vs. time data obtained, [Figure 7 C] we have observed that the photocurrent density decreases over time from 180 $\mu\text{A} / \text{cm}^2$ to 30 $\mu\text{A} / \text{cm}^2$. This further signifies that the ZnO film is not so much stable and will have to be studied further in order to prevent corrosion by tuning the electrolyte concentration and making ALD deposition of metal oxide passivation layer. These studies are not the subject of interest during the present investigation. For the time being, we have developed the proof of concept which we believe helps the ZnO nanoparticulate film to be applicable as an effective photoanode

obtained with a very cheap solution processing and dip-coating route. Here we would also like to clarify that the photocurrent density measured in case of bulk electrolysis cell [inset of Figure 7c] is slightly different from that measured in a cappuccino cell as shown in Figure 6.A. The reason for this ambiguity is not known so far.

Finally in Figure 8, we propose a real device application of the dip-coated ZnO film. As we mentioned above, it can be used as a transparent window in the rooftop of modern buildings. Here, it will perform dual actions of UV filtering and photoelectrochemical water splitting. During the PEC process, it splits the molecule of water into H₂ and O₂ with necessary bias from a photovoltaic panel and this can be finally supplied to a PEM fuel cell (not shown in the proposed scheme) for generating electricity in the household. The ZnO photoanode in this case absorbed only the UV portion of sunlight due to its band gap (3.2 eV) and it transmit the visible light into the building which can be used for lightening purpose. We would also like to state that with a newly developed protocol for large electrode fabrication [47], it will be feasible to adopt this strategy for making 10 x 10 cm² transparent ZnO electrodes. This ultimately helps in the large scale manufacturing of the electrode at an industrial scale.

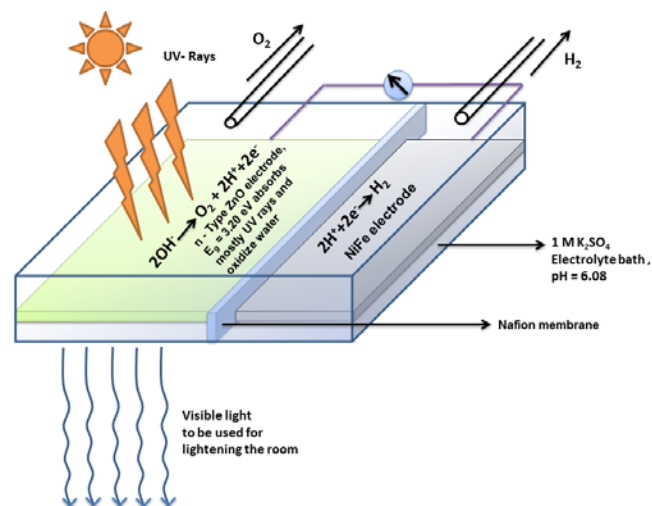


Figure 8: Proposed device with transparent nanoparticulate ZnO window panel having dual functionality of UV filter and photoelectrochemical water splitting.

Conclusions

From the above discussion, we conclude that an effective non-aqueous solution processing route has been developed for depositing transparent nanoparticulate ZnO thin film with dip-coating methodology. The optical properties of the ZnO film with different layers deposition have an absorption onset at 357 nm with exception for 2 and 3 layers deposited film. The presence of interference fringes in transmittance spectra validates the observed colour gradient on the prepared film. The band gap of the 2 layers ZnO film is found to be 3.13 eV for

direct bandgap transition and the structural properties of the ZnO film further showed the formation of nanocrystallites with hexagonal phases. The nanoparticle constituting the film have elongated shape and its average particle size found to be around 21.04 nm with the consideration of the Feret's diameter for elongated nanoparticles. The photocurrent density measurement of the optimized film (2 layers dip-coated) shows 1 mA / cm² which is quite promising for a pristine nanoparticulate ZnO film obtained in solution processed manner. The prepared electrode also shows reasonable amount of oxygen evolution which along with its transparency nature makes it applicable as transparent window for dual action of UV filtering and photoelectrochemical water splitting.

Acknowledgements

Funding for this research was provided by the Swiss Federal Office of Energy project No. 100411, the Seventh Framework Program "Novel Materials for Energy Applications" grant No. 227179 (NanoPEC – Nanostructured Photoelectrodes for Energy Conversion), and the Swiss National Science Foundation R'Equip No. 206021-121306. The spectro-electrochemical cell was built by Peter Wyss and Marc Zollinger (Empa Machine Shop) after a design provided by Laboratory for Photonics and Interfaces, EPFL Lausanne. For the development of in - situ GC set up thanks goes to Dr. Rita Toth and Dr. Krisztina- Gazda Schrantz from EMPA Dübendorf.

Notes and references

^a Laboratory for High Performance Ceramics, Empa. Swiss Federal Laboratories for Materials Science and Technology, CH- 8600, Dübendorf, Switzerland. E- mail: artur.braun@alumni.ethz.ch; Fax: +41 58 765 4150; Tel: +41 58 765 4850. E- Mail: debajeet.bora@empa.ch; Fax: +41 58 765 4150; Tel: +41 58 7654254.

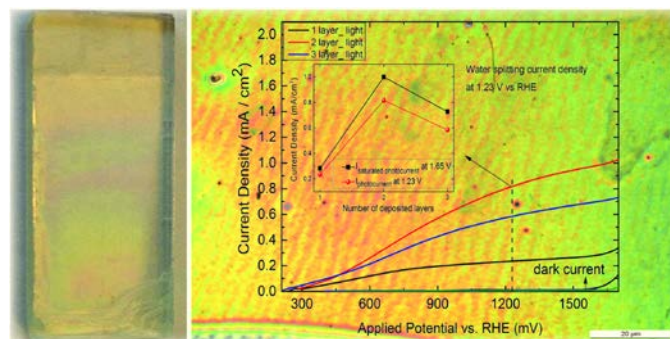
- H. J. Lewerenz, *Chem. Soc. Rev.*, 1997, **26**, 239.
- E. Becquerel, *C. R. Acad. Sci.*, 1839, **9**, 561.
- A. Fujishima and K. Honda, *Nature*, 1972, **238**, 37.
- K. L. Hardee and A. J. Bard, *J. Electrochem. Soc.*, 1976, **123**, 1024.
- W. Gaertner, *Phys. Rev.*, 1959, **116**, 84.
- H. H. Kung, H. S. Jarrett, A. W. Sleight and A. Ferretti, *J. Appl. Phys.*, 1977, **48**, 2463
- C. Klingshirm, *Chem. Phys. Chem.*, 2007, **8**, 782.
- H. Tributsch and M. Calvin, *Photochem. Photobiol.*, 1971, **14**, 95.
- X. Yang, A. Wolcott, G. Wang, A. Sobo, R. C. Fitzmorris, F. Qian, J. Z. Zhang and Y. Li, *Nano Lett.*, 2009, **9**, 2331.
- M. Guo, P. Diao and S. Cai, *Appl. Surf. Sci.*, 2005, **249**, 71.
- A. Wolcott, W. A. Smith, T. R. Kuykendall, Y. Zhao and J. Z. Zhang, *Adv. Funct. Mater.*, 2009, **19**, 1849.
- V. Srikant and D. R. Clarke, *J. Appl. Phys.*, 1998, **83**, 5447.
- Y. Yan, K. S. Ahn, S. Shet, T. Deutsch, M. Huda, S.H. Wei, J. Turner and M. M. Al-Jassim, *Proc. of SPIE*, 2007, **6650**, 66500H.
- M. A. Mansoor, M. A. Ehsan, V. McKee, N. Huang, M. Ebadi, Z. Arifin, W. J. Basiruna and M. Mazhar, *J. Mater. Chem. A*, 2013, **1**, 5284.
- S. Shet, K. Ahn, T. Deutsch and H. Wang, N. Ravindra, Y. Yan, J. Turner and M. Al-Jassim, *J. Mater. Res.*, 2010, **25**, 69.
- R. Dom, L. R. Baby, H. G. Kim and P. H. Borse, *Inter. J. Photoenerg.*, 2013, **2013**,1.
- H. M. Chen, C. K. Chen, Y. Chang, C. Tsai, R. Liu, S. Hu, W. Chang and K. Chen, *Angew. Chem. Int. Ed.*, 2010, **49**, 5966.
- K. Keis, E. Magnusson, H. Lindström, S. Lindquist and A. Hagfeldt, *Sol. Energ. Mater. Sol. C.*, 2002, **73**, 51.
- L. Bahadur, S. Kushwaha, *Appl. Phys. A*, 2012, **109**, 655.
- K. Nonomura, T. Yoshida, D. Schlettwein, H. Minoura, *Electrochim. Acta*, 2003, **48**, 3071.
- Y. Wei, L. Ke, J. Kong, H. Liu, Z. Jiao, X. Lu, H. Du and X.W. Sun, *Nanotechnology*, 2012, **23**, 235401.
- E. M. P. Steinmiller and K. Choi, *PNAS*, 2009, **106**, 20633.
- J. Schrier, D. O. Demchenko and L. Wang, *Nano Lett.*, 2007, **7**, 2377.
- H. Saarenpää, T. Niemi, A. Tukiainen, H. Lemmetyinen, N. Tkachenko, *Sol. Energ. Mat. Sol C.*, 2010, **94**, 1379.
- B. S. Ong, C. Li, Y. Li, Y. Wu and R. Loutfy, *J. Am. Chem. Soc.*, 2007, **129**, 2750.
- A. M. Schimpf, C. E. Gunthardt, J. D. Rinehart, J. M. Mayer and D. R. Gamelin, *J. Am. Chem. Soc.*, 2013, **135**, 16569.
- W. Hu, Y. Liu, Z. Zhu, H. Yang and C. M. Li, *ACS Appl. Mater. interfaces*, 2010, **2**, 1569.
- M. Behrens, F. Studt, I. Kasatkin, S. Köhl, M. Hävecker, F. Abild-Pedersen, S. Zander, F. Girgsdies, P. Kurr, B. L. Kniep, M. Tovar, R. W. Fischer, J. K. Nørskov and R. Schlögl, *Science*, 2012, **336**, 893.
- M. Grätzel, *Nature*. 2001, **414**, 338.
- S.S. Shinde, P. S. Patil, R.S. Gaikwad, R.S. Mane, B.N. Pawar, K.Y. Rajpur, *J. Alloy. Compd.*, 2010, **503**, 416.
- M. Guo, P. Diao, X. Wang and S. Cai, *J. Solid State Chem.* 2005, **178**, 3210.
- A. A. Mosquera, D. Horwat, A. Rashkovskiy, A. Kovalev, P. Miska, D. Wainstein, J. M. Albella and J. L. Endrino, *Scientific Reports*, 2013, **3**, 1714.
- (a) H. Sirringhaus, *Adv. Mater.*, 2005, **17**, 2411.; (b) C. D. Dimitrakopoulos and P. R. L. Malenfant, *Adv. Mater.*, 2002, **14**, 99. (c) B. A. Ridley, B. Nivi and J. M. Jacobson, *Science*, 1999, **286**, 746.
- K. Ellmer, A. Klein, *Transparent Conductive Zinc Oxide Basics and Applications in Thin Film Solar Cells*, Springer-Verlag, Berlin, Heidelberg, 2008.
- P. Kumar, N. Singh, A. Solanki, S. Upadhyay, S. Chaudhary, V. R Satsangi, S. Dass and R. Chemistry of

Phytopotentials: Health, Energy and Environmental Perspectives, Springer-Verlag Berlin, Heidelberg 2012.

36. M. A. Kats, S. J. Byrnes, R. Blanchard, M. Kolle, P. Genevet, J. Aizenberg, and F. Capasso, *Appl. Phys. Lett.* 2013, **103**, 101104.
37. D. K. Bora, A. Braun, S. Erat, A. K. Ariffin, R. Loehnert, K. Sivula, J. Toepfer, M. Graetzel, R. Manzke, T. Graule and E. C. Constable, *J. Phys. Chem. C*, 2011, **115**, 5619
38. J. Tauc, R. Grigorov, A. Vancu, *Phys. Status Solidi*, 1966, **15**, 627
39. R. B. Heller, J. McGannon, A. H. Weber, *J. Appl. Phys.*, 1950, **21**, 1283.
40. W. H. Walton, *Nature*, 1950, **162**, 329-330.
41. W. B. Ingler, J. P. Baltrus and S. U. M. Khan, *J. Am. Chem. Soc.*, 2004, **126**, 10238.
42. J. Cao, T. Kakoi, N. Kikugawa and Jinhua Ye, *J. Phys. D: Appl. Phys.* 2010, **43**, 325101.
43. a. Y. V. Pleskov, A. Y. Sakharova, M. D. Krotova, L. L. Bouilov and B. V. Spitsyn, *J. Electroanal. Chem.*, 1987, 228, 19; b. Y. V. Pleskov and Y. Y. Gurevich, *semiconductor photoelectrochemistry*, Consultants Bureau, New York, 1986.
44. C. M. Eggleston, A. J. A. Shankle, A. J. Moyer, I. Cesar and M. Gratzel, *Aquat. Sci.* 2009, **71**, 151.
45. P. Iwanski, J. S. Curran, W. Gissler and R. Memming, *J. Electrochem. Soc.*, 1981, **128**, 2128.
46. D. K. Bora, A. Braun, R. Erni, G. Fortunato, T. Graule and E. C. Constable, *Chem. Mater.* 2011, **23**, 2051-2061.
47. Y. Hu, D. K. Bora, F. Boudoire, F. Häussler, M. Graetzel, E. C. Constable, A. Braun, *J. Ren. Sustain. Energ.* 2013, **5**, 043109.
48. S. Shet, *ECS Trans.* 2011, **33**, 15.
49. V. S. Thoi, H. I. Karunadasa, Y. Surendranath, J. R. Long C. J. Chang, *Energ. Environ. Sci.*, 2012, **5**, 7762.

¹ From the photoelectrochemical investigation, no significant photocurrent has been observed for hematite film deposited by spin coating of the polymeric precursor. This negative influence is attributed to the less porous character of the film along with very smooth surface. It is to be noted that only film having precise roughness are found to be very photoactive.

TOC



A solution processed synthetic route has been developed for making transparent ZnO thin film having nanoparticle size of 21.04 nm. Without additional modification ZnO films shows current density of 1mA / cm². The films also exhibit the production of oxygen gas from photo electrochemical water oxidation.